

# From Target Tracking to Targeting Track — Part I: A Metric for Spatio-Temporal Trajectory Evaluation

Tiancheng Li, *IEEE Senior Member*, Yan Song, Hongqi Fan, Jingdong Chen, *IEEE Fellow*

**Abstract**—In the realm of target tracking, performance evaluation plays a pivotal role in the design, comparison, and analytics of trackers. Compared with the traditional trajectory composed of a set of point-estimates obtained by a tracker in the measurement time-series, the trajectory that our series of studies including this paper pursued is given by a curve function of time (FoT). The trajectory FoT provides complete information of the movement of the target over time and can be used to infer the state corresponding to arbitrary time, not only at the measurement time. However, there are no metrics available for comparing and evaluating the trajectory FoT. To address this lacuna, we propose a metric denominated as the spatio-temporal-aligned trajectory integral distance (Star-ID). The Star-ID associates and aligns the estimated and actual trajectories in the spatio-temporal domain and distinguishes between the time-aligned and unaligned segments in calculating the spatial divergence including false alarm, miss-detection and localization errors. The effectiveness of the proposed distance metric and the time-averaged version is validated through theoretical analysis and numerical examples of a single target or multiple targets.

**Index Terms**—Tracker performance evaluation, target tracking, trajectory function of time, distance metric.

## I. INTRODUCTION

MULTI-target tracking (MTT) is an intricate process that entails the sequential estimation of both the cardinality (number of targets) and the kinematic states of multiple targets, where both parameters are potentially time-variant [1], [2], [3]. It has been a key technology in the applications of autonomous driving, guidance and defense systems, traffic control, and robotics. Typically, each target is assigned a unique identification, and the output of the tracking algorithm is manifested as distinguishable temporal sequences of state estimates, referred to as tracks [4], [5], [6], [7]. Quantifying the similarity between the ground truth and estimated tracks [8], [9], [10], the core for performance evaluation, which needs to grapple with significant ambiguities [11] holds paramount significance in the design, comparison, and analytics of any tracker [12], [13], [14]. Irrespective of the choice of tracking

Manuscript created August 2024;

This work was supported in part by the National Natural Science Foundation of China under Grants 62422117 and 62201316 and in part by the Fundamental Research Funds for the Central Universities.

Tiancheng Li and Yan Song are with the Key Laboratory of Information Fusion Technology (Ministry of Education), School of Automation, Northwestern Polytechnical University, Xi'an 710129, China, E-mail: t.c.li@nwpu.edu.cn, syz@nwpu.edu.cn. Hongqi Fan is with the College of Electronic Science and Technology, National University of Defense Technology, Changsha 410073, China, E-mail: fahongqi@nudt.edu.cn. Jingdong Chen is with the School of Marine Science and Technology, Northwestern Polytechnical University, Xi'an 710129, China, E-mail: jingdongchen@ieee.org.

algorithms, the metric plays an essential role in the performance evaluation. Arguably, different metrics or even different parameter choices will all lead to diverse results [15].

### A. Relevant Work

The most widely used metric for multi-target estimate evaluation is the so-called optimal sub-pattern assignment (OSPA) distance [16]. This metric extends the Wasserstein metric to the general case where two point-sets may have different numbers of points. It comprises two components, referred to as the localization error and cardinality/quantity error; the latter accounts for the false alarm (FA) and missed detection (MD), which are two notable challenging issues for MTT. A meaningful extension of this approach is to incorporate the uncertainty of each point-estimate [17]. Relevantly, the target existence probability taken as the track quality information is accounted for within the OSPA in [18]. Furthermore, the negative log-likelihood of the posterior that incorporates all uncertainties is defined as a measure [19]. The OSPA metric has inspired many other metrics such as the generalized OSPA (GOSPA) [20], [21], and complete OSPA (COSPA) [10], among others [22], [23].

However, calculating the estimation error at each sampling step in isolation is inadequate for tracker evaluation. Instead, the metric should account for the dissimilarity between the overall tracks consisting of time-series of point-estimates [24], [25], [15] or of sub-densities [7]; see a substantial body of work reviewed in [26], [27], [15]. This line of thought leads to the foundation of the metric of OSPA<sup>(2)</sup> [28], [25], which is a spatio-temporal metric that accounts for both the spatial and temporal information of the tracks. Notably, the metric proposed in [24] allows trajectory association to be changed over time and incorporates the confusion of trajectories' identity in an optimal way. Nonetheless, these OSPA-like metrics are predominantly designed for use with traditional recursive filters/trackers where the estimates are obtained in discrete measurement time series and so the evaluation deals with point-state estimates obtained in time series as illustrated in Fig. 1 (a) and (b). They are not applicable to the continuous-time trajectory case—with the exception that the metric proposed in [24] is claimed, yet not validated, to have the potential for extension to continuous time – where each trajectory is given by a continuous-time curve as shown in Fig. 1 (c), not a set of points obtained in discrete time series. Although there are a large number of studies on continuous-time state estimation [29], there is to date no metric available for general continuous-time trajectories except for our preliminary work [30] as to be explained in this paper.

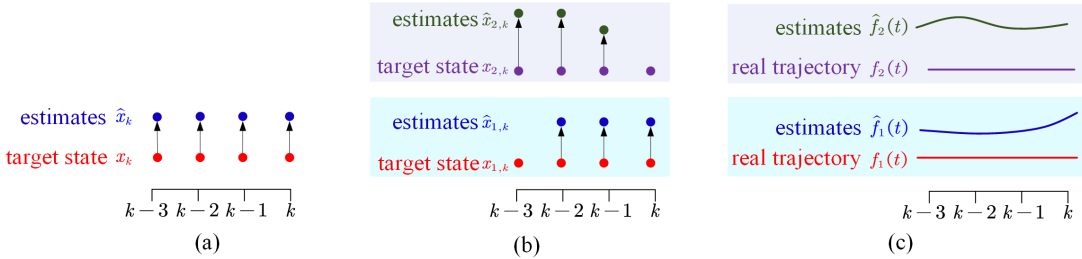


Fig. 1. Different tracking scenarios: (a) single target point-state estimation; (b) multiple target point-state estimation; (c) multi-target T-FoT estimation.

### B. Introduction to Companion Papers

Our series of studies are founded on modeling the target trajectory using a curve function of time (FoT) as shown in Fig. 1 (c), which was termed the trajectory FoT (T-FoT) [31], [32]. That is, the evolution of the target state over time is modeled by T-FoT  $f : \mathbb{R}^+ \rightarrow \mathcal{X}$  in the spatio-temporal space and the target state at time  $t$  is given by

$$\mathbf{x}_t = f(t), \quad (1)$$

where  $t \in \mathbb{R}^+$  denotes the time and  $\mathcal{X}$  denotes the state space.

Specifically, the T-FoT can be given in the forms of a polynomial [31], [32] (see also the companion paper [33]), B-spline basis functions [34] and so on [35]; see the review given in [29]. That being said, the metric we seek in this paper is unlimited to any specific form but applicable for the general continuous-time case. Most existing studies, however, do not provide uncertainty about their T-FoT estimate. Moreover, they fail to utilize any information regarding the state correlation over time. To put it simply, the states corresponding to close time instants are more likely to be in closer spatial proximity to each other than those far away. To take advantage of this latent state temporal correlation and to provide an assessment of the uncertainty associated with the T-FoT estimate, within our series of companion papers [33], [36] we further model the collection of the target state as a stochastic process (SP)  $\mathcal{F} \triangleq \{\mathbf{x}_t : t \in \mathbb{R}^+\}$  defined on the continuous time. That is, any particular T-FoT is a sample path of this SP, i.e.,

$$f(t) \sim \mathcal{F}. \quad (2)$$

The contributions of our series of companion papers including three parts are structured as follows.

- This paper, which serves as Part I of this series of papers, proposes a metric for evaluating the quality of any T-FoT estimate  $\hat{f}$ . This provides a distance measure between any two trajectories represented in the form of an FoT. To avoid distracting the reader's attention from our key contribution, this paper will not delve further into the SP model but focus only on the T-FoT metric.
- Part II [33] and Part III [36] offer solutions to online learning of the SP via decomposing it into a deterministic FoT and the residual SP according to some decomposition approaches [37], [38]. The former fits the trend of the trajectory by the best polynomial FoT based on regularized optimization while the latter approximates the residual SP by two representative SPs: the Gaussian process (GP) and Student's  $t$  process (StP).

### C. Contribution and Organization of This Paper

From both theoretical and practical perspectives, a metric capable of appropriately measuring the similarity of continuous-time T-FoTs that can be arbitrary forms is of vital importance for analyzing and comparing the performance of these trackers and for evaluating different strategies for algorithm improvement. In addition, it is required for multi-sensor cooperation and fusion in order to determine the correspondence between trajectories obtained by different sensors. Such a metric that is mathematically rigorous and meets the need of multiple spatio-temporal T-FoT evaluation constitutes the contribution of this paper.

The remainder of this paper is organized as follows. Existing representative MTT metrics are briefly reviewed in Section II. Section III discusses the elemental distance/metric to be utilized in the proposed T-FoT metric, referred to as the spatio-temporal-aligned trajectory integral distance (Star-ID), which is given later in Section IV. Scenario study is given in Section V before the paper is concluded in Section VI. The main notations used in this paper are given in Table I.

TABLE I  
LIST OF KEY NOTATIONS

Notation	Interpretation
$t$	$t \in \mathbb{R}^+$ , the continuous time (positive real number)
$\mathcal{F}$	stochastic process of the state
$\mathbf{x}_k$	the target state at time $k$
$k$	$k \in \mathbb{N}^+$ , the discrete sampling time (integer)
$\mathbf{y}_k$	the measurement at time $k$
$h_k(\cdot)$	the measurement function at time $k$
$\mathbf{v}_k$	the measurement noise at time $k$
$f(t), g(t)$	the (real or estimated) target T-FoTs
$F(t; \mathbf{C})$	a polynomial T-FoT with parameters $\mathbf{C}$
$\mathbf{C}$	set of polynomial parameters $\mathbf{C} = \{\mathbf{c}_0, \mathbf{c}_1, \dots, \mathbf{c}_\gamma\}$
$\gamma$	the order of the T-FoT function
$T_w$	the maximum length of the sliding time-window
$r$	the trajectory dimension
$c$	the cutoff coefficient for OSPA and OSPA <sup>(2)</sup>
$p$	the metric order for OSPA, OSPA <sup>(2)</sup> and Star-ID
$c_{\text{CSFA}}, c_{\text{SMD}}$	segment cutoff coefficient for FA and MD, respectively
$T_{\text{SFA}}, T_{\text{SMD}}$	duration of the segment FA and MD, respectively
$c_{\text{CTFA}}, c_{\text{CTMD}}$	trajectory cutoff coefficient for FA and MD, respectively
$T_{\text{CTFA}}, T_{\text{CTMD}}$	duration of the trajectory FA and MD, respectively

## II. PRELIMINARIES

In this section, we will briefly review the OSPA-type metrics for point sets and our previous related work.

### A. OSPA: Metric on Sets of Points

The widely used OSPA distance [16] measures the distance between two sets of points which adds consideration of the cardinality inconsistency to the Wasserstein metric. For  $\Phi = \{\phi^{(1)}, \phi^{(2)}, \dots, \phi^{(m)}\}$  and  $\Psi = \{\psi^{(1)}, \psi^{(2)}, \dots, \psi^{(n)}\}$ , with  $m \leq n$ , the OSPA distance with order  $p$  and cutoff coefficient  $c$  is defined as follows

$$\text{OSPA}_p^{(c)}(\Phi, \Psi) = \left( \frac{1}{n} \left( \min_{\pi \in \prod_n} \sum_{i=1}^m \check{d}^{(c)}(\phi^{(i)}, \psi^{(\pi(i))})^p + c^p(n-m) \right) \right)^{\frac{1}{p}}, \quad (3)$$

where  $\check{d}^{(c)}(\phi^{(i)}, \psi^{(i)}) \triangleq \min(c, d(\phi^{(i)}, \psi^{(i)}))$ , in which  $d(\cdot, \cdot)$  is a metric on the single-target state space. If  $m > n$ , then  $d_p^{(c)}(\Phi, \Psi) = d_p^{(c)}(\Psi, \Phi)$ .

### B. Unnormalized OSPA and GOSPA

As shown, the OSPA is a normalized metric which, however, suffers from an obvious drawback as mentioned by the creators [16] that it is insensitive to the case where one is empty. In other words, when one set is empty, the OSPA distance takes on the cutoff value of  $c$  regardless of the cardinality of the other set. Another issue with the OSPA metric as pointed out by [20] is that it gives the same result  $c$  for the distance between two sets  $\Phi$  and  $\Psi$  where  $|\Psi| = |\Phi| - 1$ , and between two sets  $\Phi$  and  $\Psi \cup z$  where  $d(x, z) \geq c$  for  $z \notin \Psi$  and  $\forall x \in \Phi$ . Yet, this can be simply resolved by the removal of the normalization, the multiplier  $\frac{1}{n}$ , resulting in the unnormalized OSPA, which is proportional to the COSPA given in [10]. By further adding parameter  $\alpha$  as a denominator in the cardinality error, one gets the GOSPA [20], [21], c.f., (3)

$$\text{GOSPA}_p^{(c)}(\Phi, \Psi) = \left( \min_{\pi \in \prod_n} \sum_{i=1}^m \check{d}^{(c)}(\phi^{(i)}, \psi^{(\pi(i))})^p + \frac{c^p}{\alpha}(n-m) \right)^{\frac{1}{p}}. \quad (4)$$

Differently from the OSPA that is a per-target error, the GOSPA is an unnormalized metric which sums up all distances between the finite sets and increases with the increase of the sizes of the sets. Sensitivity of the OSPA and GOSPA metrics to the parameters has been analyzed in [39].

### C. OSPA<sup>(2)</sup>: Metric on Sets of Tracks

The so-called OSPA<sup>(2)</sup> metric [28], [25] measures the distance between two sets of tracks which does not only capture target state errors, cardinality errors, but also phenomena such as track switching and track fragmentation. Here, each track is a time-series of point-estimates as shown in Fig. 1 (b).

Consider two set of tracks  $\mathbf{X} = \{\Phi^{(1)}, \Phi^{(2)}, \dots, \Phi^{(m)}\}$  and  $\mathbf{Y} = \{\Psi^{(1)}, \Psi^{(2)}, \dots, \Psi^{(n)}\}$ , where each track  $\Phi^{(i)}$  or  $\Psi^{(j)}$  consists of a time-series of points,  $1 \leq i \leq m, 1 \leq$

$j \leq n$ . Assuming  $m \leq n$ , the OSPA<sup>(2)</sup> distance  $d_{p,q}^{(c,w)}(\mathbf{X}, \mathbf{Y})$  between  $\mathbf{X}$  and  $\mathbf{Y}$  is defined as

$$\text{OSPA}_{p,q}^{(2)(c,w)}(\mathbf{X}, \mathbf{Y}) = \left( \frac{1}{n} \left( \min_{\pi \in \prod_n} \sum_{i=1}^m \tilde{d}_q^{(c,w)} \left( \Phi^{(i)}, \Psi^{(\pi(i))} \right)^p + c^p(n-m) \right) \right)^{\frac{1}{p}} \quad (5)$$

where  $q$  is the order of the base distance, all positive-defined and  $\tilde{d}_q^{(c,w)}(\Phi, \Psi)$  between two tracks  $\Phi, \Psi$  is defined as

$$\tilde{d}_q^{(c,w)}(\Phi, \Psi) = \left( \sum_{t=1}^K \left( w(t) d^{(c)}(\{\Phi(t)\}, \{\Psi(t)\}) \right)^q \right)^{\frac{1}{q}} \quad (6)$$

where  $w(t) > 0$  is a positive weighting function defined for  $t \in \{1, \dots, K\}$  which includes all time indices from the beginning to the end of the tracking scenario, such that  $\sum_{t=1}^K w(t) = 1$  and the singleton-based OSPA distance reduces to the following

$$d^{(c)}(\phi, \psi) = \begin{cases} 0, & |\phi| = |\psi| = 0 \\ c, & |\phi| \neq |\psi| \\ \min(c, d(\phi, \psi)), & |\phi| = |\psi| = 1 \end{cases} \quad (7)$$

Note that  $d_{p,q}^{(c,w)}(\mathbf{X}, \mathbf{Y}) = d_{p,q}^{(c,w)}(\mathbf{Y}, \mathbf{X})$  if  $m > n$ . While the OSPA distance indicates the per-target error, the OSPA<sup>(2)</sup> distance can be interpreted as the time-averaged per-track error. In both, smaller values indicate higher accuracy.

### D. Integral Multi-target Trajectory Assignment (IMTA) Metric

An intuitive approach to the T-FoT evaluation is discretizing the continuous-time curve function into discrete points and using established metrics such as the OSPA<sup>(2)</sup> for evaluation. This, however, will cause the loss of detailed information of the trajectory, such as the length and smoothness, and loss of the advantage of obtaining the whole trajectory. For example, this approach can not distinguish the two different trajectory estimates shown in Fig. 2 and therefore undermines the purpose of performance evaluation metric. Instead, we need to directly calculate the distance between two sets of continuous-time functions.

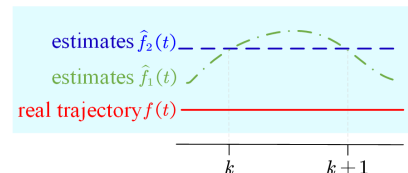


Fig. 2. Two different T-FoTs share the same discretizing points.

Our earlier attempt as called the IMTA metric in [30] is first reviewed. Let  $\mathcal{F} = \{f_1, f_2, \dots, f_m\}$  and  $\mathcal{G} = \{g_1, g_2, \dots, g_n\}$  be finite subsets of continuous-time T-FoTs of size  $m$  and

$n$ , respectively, one being the ground truth and the other estimates. If  $m \leq n$ , the IMTA metric is defined as

$$\text{IMTA}_r^{(c)}(\mathcal{F}, \mathcal{G}) = \min_{\pi \in \Pi_n} \left( \sum_{i=1}^m d_r^{(2)}(f_i, g_{\pi(i)}) + (c_{\text{TFA}} T_{\text{TFA}} + c_{\text{TMD}} T_{\text{TMD}})^r \right), \quad (8)$$

where  $T_{\text{TFA}}$  and  $T_{\text{TMD}}$  denote the duration time of the false and missed trajectories, and  $c_{\text{TFA}}$  and  $c_{\text{TMD}}$  are the corresponding penalty in two cases, respectively, and the pairwise distance  $d_r^{(2)}(f, g)$  between two T-FoTs  $f, g$  is as follows

$$d_r^{(2)}(f, g) = \frac{1}{\tau} \left( d_{t_1, t_2}^{(2)}(f, g) + (c_{\text{SFA}} T_{\text{SFA}} + c_{\text{SMD}} T_{\text{SMD}})^r \right), \quad (9)$$

where  $t_1, t_2$  indicate the starting and ending times of the common time domain of the two T-FoTs  $f, g$ , respectively,  $\tau = (t_2 - t_1 + T_{\text{SFA}} + T_{\text{SMD}})^r$ ,  $T_{\text{SFA}}$  and  $T_{\text{SMD}}$  denote the duration time of the FA and MD, and  $c_{\text{SFA}}$  and  $c_{\text{SMD}}$  are the corresponding FA and MD penalty, respectively,  $d_{t_1, t_2}^{(2)}(f, g)$  is the  $\ell_2$  distance between two functions  $f$  and  $g$  in the common time domain  $[t_1, t_2]$ , c.f. (11)

$$d_{t_1, t_2}^{(2)}(f, g) = \int_{t_1}^{t_2} (f(t) - g(t))^T (f(t) - g(t)) dt. \quad (10)$$

As shown above, the pairwise distance between associated trajectories is defined by the integral of the divergence of two functions, whether  $\ell_1$  or  $\ell_2$  norms, over time. The unit of the metric is spatio-temporal such as  $\text{m} \cdot \text{s}$ . This is significantly different from the metric for point sets. The IMTA metric, however, has two limitations and drawbacks:

- IMTA does not properly coordinate the localization error and FA/MD error since in the former the error in each dimension is summarized while in the latter it is accounted for by the exponential calculation. Two parts have different units of error unless  $r = 1$ . This theoretical drawback can be fixed by substituting the exponential calculation in the latter with multiplication.

We next propose a new spatio-temporal metric that overcomes the above limitations and drawbacks.

### III. ELEMENTAL SEGMENT DISTANCE

Similar to the distance between point sets, the distance between T-FoT sets that needs to solve the trajectory-to-trajectory (T2T) association problem first. But differently, the T-FoT association needs to be carried out in the continuous time domain and both the trajectory FA/MD (TFA/TMD) and segment FA/MD (SFA/SMD) are defined too in the continuous time domain. More formally speaking,

- *Trajectory temporal-alignment*: The T-FoT divergence needs to account for the temporal overlap and non-overlap parts, separately. The former constitutes the spatial difference between the temporally aligned T-FoT segments while the latter constitutes the SFA or SMD, namely unaligned segment error. As a result, two T-FoTs that overlap spatially but not temporally are different as illustrated in Fig. 3.

- *FA and MD errors*: The FA and MD are not solely determined by a simple disparity in the number of tracks (i.e., TFA/TMD) but also by the trajectory non-overlap/unaligned segments (i.e., SFA/SMD). In addition, both cases need to take into account the duration of the concerning FA/MD. For instance, the cost of missing a track (or a segment) spanning 1s is evidently different from that spanning 5s<sup>1</sup>. In an extreme case when the duration of the MD is so short that it is less than a sampling period as shown in Fig. 4, no existing point-estimate metric can properly calculate the MD error. In the T-FoT approach, the penalty for FA and MD needs to take into account the duration.



Fig. 3. Two T-FoT estimates overlap spatially but not temporally.

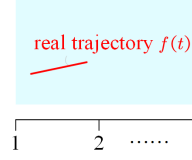


Fig. 4. A target exists less than a sampling period and is undetected by the estimator.

Therefore, the first step to calculate the distance between two trajectories is to divide them into segments in the time domain according to their temporal alignment. The second step is to calculate the spatio-temporal-domain-based distance with regard to each segment, which forms the elemental units to construct our final metric for T-FoT comparison.

#### A. Temporally Aligned Segment

We define the spatio-temporal distance between two temporally aligned segments as follows.

**Definition 1** ( $\ell_p$  distance). *The  $\ell_p$  distance of two T-FoTs  $f, g$  in the same time interval  $[t_1, t_2]$  is defined as*

$$d_{t_1, t_2}^{(p)}(f, g) \triangleq \int_{t_1}^{t_2} \|f(t) - g(t)\|_p dt, \quad (11)$$

where the  $\ell_p$  norm is defined as  $\|\mathbf{x}\|_p \triangleq (\sum_{i=1}^r |\mathbf{x}[i]|^p)^{\frac{1}{p}}$ .

#### B. Temporally Unaligned Segment: SFA/SMD

SFA refers to the estimated trajectory segment that is not assigned to any real trajectory. The SFA duration corresponding to the time-window  $[t_{\text{SFA},1}, t_{\text{SFA},2}]$  is given by

$$T_{\text{SFA}} = t_{\text{SFA},2} - t_{\text{SFA},1}. \quad (12)$$

<sup>1</sup>Similar issue has been overlooked in existing track metrics such as the OSPA<sup>(2)</sup> distance in which, as shown in (5), each FA or MD is recognized the same as error  $c$  in the result, no matter how long each FA or MD exists.

SMD refers to the real trajectory segment that is not assigned to any estimated trajectory. The SMD duration corresponding to the time-window  $[t_{\text{SMD},1}, t_{\text{SMD},2}]$  is given by

$$T_{\text{SMD}} = t_{\text{SMD},2} - t_{\text{SMD},1}. \quad (13)$$

Correspondingly, penalty should be applied to the SFA and SMD by using the segment cutoff coefficients  $c_{\text{SFA}}$  and  $c_{\text{SMD}}$ , respectively. Similarly, we denote the duration and cutoff coefficients for the TFA and TMD by  $T_{\text{TFA}}$ ,  $c_{\text{TFA}}$  and  $T_{\text{TMD}}$ ,  $c_{\text{TMD}}$ , respectively. A longer duration and a higher penalty will indicate a greater distance between the estimated and real trajectories. Note that these cutoff parameters should not be arbitrarily chosen but follow certain rules as to be addressed in section IV.B.

### C. Distance between Two T-FoTs

A convincing distance between two sets of T-FoTs has to be built on the base of a meaningful base-distance between two single T-FoTs. After temporally aligning the estimated and actual T-FoTs  $f, g$ , the spatio-temporal distance can be defined as follows:

$$d_c^{(p)}(f, g) = \left( r(c_{\text{SFA}}T_{\text{SFA}} + c_{\text{SMD}}T_{\text{SMD}})^p + d_{t_1, t_2}^{(c, p)}(f, g) \right)^{1/p}, \quad (14)$$

where

$$d_{t_1, t_2}^{(c, p)}(f, g) \triangleq \min \left( (d_{t_1, t_2}^{(p)}(f, g))^p, r(c_{\text{SFA}} + c_{\text{SMD}})^p(t_2 - t_1)^p \right). \quad (15)$$

Here,  $[t_1, t_2]$  denotes the aligned time interval of  $f$  and  $g$ ,  $p$  represents the metric order s.t.  $1 \leq p < \infty$ , the parameter  $r$  scales the distance with the dimension of the trajectory in order to comply with the  $\ell_p$  norm in (11).

**Definition 2** (Distance metric). *Given a metric  $d(\cdot, \cdot)$  and any three items  $f, g$  and  $h$ ,  $d$  is a distance metric if it has the following four properties:*

- 1) non-negativity:  $d(f, g) \geq 0$
- 2) identity:  $d(f, g) = 0 \iff f(t) = g(t)$
- 3) symmetry:  $d(f, g) = d(g, f)$
- 4) triangle inequality:  $d(f, g) \leq d(f, h) + d(h, g)$

**Theorem 1.** *When  $c_{\text{SFA}} = c_{\text{SMD}} > 0$  and  $1 \leq p < \infty$ ,  $d_c^{(p)}(f, g)$  is a distance.*

*Proof.* Following Definition 2, the proof is given in Appendix VI-B.  $\square$

**Remark 1.** *When there are multiple trajectories in either the estimated or actual T-FoT set, the T2T association is needed to calculate the distance. Different association results lead to different  $T_{\text{TFA}}, T_{\text{TMD}}, T_{\text{SFA}}$  and  $T_{\text{SMD}}$ . Therefore, we hereafter write these parameters more formally by  $T_{\text{TFA}}^\theta, T_{\text{TMD}}^\theta, T_{\text{SFA}}^\theta, T_{\text{SMD}}^\theta$ , where  $\theta$  denotes the global T2T association between the estimated and actual T-FoT sets. Once the pairwise T-FoT distance is properly defined like in (14), one can solve the T2T association problem between two sets of T-FoTs by using methods such as the known Hungarian/Kuhn-Munkres algorithm [40].*

### IV. PROPOSED METRIC: STAR-ID

Integrating the pairwise distance between two T-FoTs with the FA and MD errors, we proceed to give the final multi-target T-FoT metric and interpret all user-specific parameters.

#### A. Main Result

Without loss of generality, let  $\mathcal{F} = \{f_1, f_2, \dots, f_m\}$  and  $\mathcal{G} = \{g_1, g_2, \dots, g_n\}$  be the real and estimated T-FoT sets. Note that in online use of the metric, one may consider merely the part of these T-FoTs in the sliding time-window used for T-FoT estimation. Furthermore, let us use  $\Theta$  to represent the set of all possible T2T associations. If  $f \in \mathcal{F}$  is associated with  $g \in \mathcal{G}$  in the global T2T association  $\theta \in \Theta$ , we define that  $\mathbf{1}_\theta(f, g) = 1$ . Otherwise,  $\mathbf{1}_\theta(f, g) = 0$ . The proposed Star-ID metric is formally defined as follows

$$d_c^{(p)}(\mathcal{F}, \mathcal{G}) = \min_{\theta \in \Theta} \left( \sum_{i=1}^n r(c_{\text{TFA}} T_{\text{TFA},i}^\theta)^p + \sum_{j=1}^m r(c_{\text{TMD}} T_{\text{TMD},j}^\theta)^p + \sum_{j=1}^m \sum_{i=1}^n \mathbf{1}_\theta(f_j, g_i) \left( \check{d}_c^{(p)}(f_j, g_i) \right)^p \right)^{1/p} \quad (16)$$

$$\text{s.t. } \sum_{j=1}^m \mathbf{1}_\theta(f_j, g_i) \leq 1, \forall 1 \leq i \leq n, \quad (17)$$

$$\sum_{i=1}^n \mathbf{1}_\theta(f_j, g_i) \leq 1, \forall 1 \leq j \leq m. \quad (18)$$

where

$$\begin{aligned} \check{d}_c^{(p)}(f, g) &= \min \left( d_c^{(p)}(f, g), (r(c_{\text{TFA}} T_g)^p + r(c_{\text{TMD}} T_f)^p)^{\frac{1}{p}} \right). \end{aligned} \quad (19)$$

Here, (17) and (18) ensure injective T2T association.

**Theorem 2.** *When  $c_{\text{SFA}} = c_{\text{SMD}} > 0, c_{\text{TFA}} = c_{\text{TMD}} > 0$  and  $1 \leq p < \infty$ ,  $d_c^{(p)}(\mathcal{F}, \mathcal{G})$  is a distance.*

*Proof.* Similar to the proof of Theorem 1, the proof of the four properties of  $d_c^{(p)}(\mathcal{F}, \mathcal{G})$  is given in Appendix VI-C.  $\square$

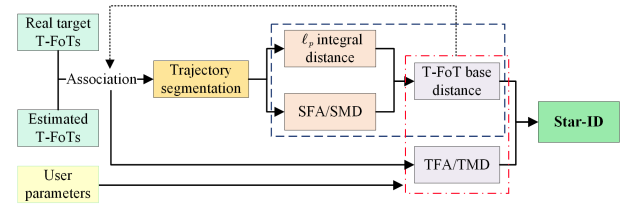


Fig. 5. Flowchart for calculating the Star-ID metric.

**Remark 2.**  *$c_{\text{SFA}} = c_{\text{SMD}} > 0$  and  $c_{\text{TFA}} = c_{\text{TMD}} > 0$  are necessary for the Star-ID to be a distance. However, in practice one may use different penalties for FA and MD although this will go against with the definition of a distance.*

As shown in (16), the Star-ID calculates the distance between two T-FoT sets, summing up the distances between all associated trajectories and the FA and MD errors over all time.

Based on this measure, we further define the time-averaged Star-ID (of spatial measure unit) as follows

**Definition 3** (Time-averaged Star-ID).

$$\bar{d}_c^{(p)}(\mathcal{F}, \mathcal{G}) \triangleq \frac{1}{k - k'} d_c^{(p)}(\mathcal{F}, \mathcal{G}) \quad (20)$$

where  $k'$  and  $k$  denote the starting and ending time of a specified time-window for evaluation, respectively.

**Remark 3.** In comparing with the normalized metrics such as OSPA and OSPA<sup>(2)</sup>, the proposed Star-ID like the GOSPA [20], [21] is unnormalized and will increase basically with the increase of the size of the T-FoT sets. This is reasonable since the more targets/estimates are involved, the higher cumulative error the tracker is supposed to have. The time-averaged Star-ID (TA-Star-ID) calculates the Star-ID per time unit, which evaluates the increase rate of the Star-ID over time, demonstrating the average instantaneous performance of the tracker. That being said, one may consider dividing the error by the number of targets (or that of the T-FoT estimates) for normalization. This, however, will not work since different FA and MD trajectories/segments may correspond to different durations and the FA/MD penalties depend on their duration. As such, FA and MD are no more a simple cardinality mismatch issue. This is a significant difference of the spatio-temporal metric with the spatial metric.

## B. Interpreting Parameters

1) *cut-off parameters*: The segment cutoff coefficients  $c_{SFA}$  and  $c_{SMD}$  emphasize the discrepancies per time unit between matched trajectory pairs, whereas the trajectory cutoff coefficients  $c_{TFA}$  and  $c_{TMD}$  are designed to penalize the errors per time unit arising from unmatched trajectories due to incorrect or absent estimates. As addressed,  $c_{SFA} = c_{SMD} > 0$  and  $c_{TFA} = c_{TMD} > 0$  are necessary for the Star-ID to be a distance. In this case, we refer to  $c_{SFA} = c_{SMD} = c_S$  by default as the segment cutoff coefficient and  $c_{TFA} = c_{TMD} = c_T$  by default as the trajectory cutoff coefficient. They are defined in the Euclid state space. Let us reconsider actual T-FoT set  $\mathcal{F} = \{f_1, f_2, \dots, f_m\}$ , estimated T-FoT set  $\mathcal{G} = \{g_1, g_2, \dots, g_n\}$  and the global T2T association  $\theta \in \Theta$ .

Moreover, typically,  $c_{TFA} \geq c_{SFA}$ ,  $c_{TMD} \geq c_{SMD}$  to ensure that missing a whole trajectory is at least more serious than missing a part of it and wrongly estimating an FA trajectory is at least more serious than obtaining an FA segment.

2) *Distance Order*: The role of the distance order  $p$  in the Star-ID is similar to that in OSPA, GOSPA and OSPA<sup>(2)</sup>. The value of  $p$  determines the sensitivity of  $d_c^{(p)}(\cdot, \cdot)$  to outlier estimates. We emphasize here two important choices. By using  $p = 1$ , the Star-ID metric measures a first-order error in which the sum of the integral distance and FA and MD error equals the total metric. In contrast,  $p = 2$  will penalize the outliers more significantly, leading to a smoother distance curve.

## V. SIMULATION STUDY

In the simulation study, the proposed Star-ID and TA-Star-ID metrics will be demonstrated basing on the T-FoT approach

to tracking in both single and multiple target scenarios. In the former, the ground truth trajectory is generated by using a traditional state space model while in the latter, they are generated directly by curve functions in the Cartesian coordinate. For the purpose of comparison, we need to find the T-FoT of the ground truth for calculating the Star-ID and TA-Star-ID in the former scenario while in the latter we need to discretize the continuous curve trajectories into discrete points at each the measuring time instant for calculating the OSPA and OSPA<sup>(2)</sup>. Perfect point-to-trajectory association is assumed in OSPA<sup>(2)</sup>. For both Star-ID and TA-Star-ID, the segment/trajectory cutoff coefficients for FA and MD are set equal, namely  $c_{SFA} = c_{SMD} = c_S$ ,  $c_{TFA} = c_{TMD} = c_T$ . We will test different cutoff parameters in two scenarios. The metric order for OSPA, OSPA<sup>(2)</sup> and Star-ID is chosen the same as  $p = 2$ . Both the Sart-ID and TA-Star-ID at time  $k$  are calculated over the sliding time-window  $K = [k', k]$  with  $k' = \max(1, k - 10)$ . In other words, the trajectories are compared only in the current time-window part. We add that the Star-ID and TA-Star-ID metrics have also been used in the companion paper [33] for multi-target T-FoT estimator evaluation.

### A. Single Maneuvering Target

The maneuvering target tracking scenario was provided in Section 4.2.2 of [41] and as shown in Fig. 6. Two Markov models were assumed for modeling the target movement with sampling step size 0.1s. The first is given by a single linear Wiener process velocity model [2] with insignificant process noise (zero-mean and power spectral density 0.01). The other is given by a combination of it with a nonlinear CT model (using no position and velocity noise but zero-mean Gaussian turn rate noise with covariance 0.15).

The bearing observation is made on the position  $[p_{x,k}, p_{y,k}]^T$  of the target, which was given by four sensors located around the four corners of the scenario. The sensors are synchronous, having the same sampling step size 0.1s. The simulation is carried out for 100 runs, each lasting 100s. The observation function of sensor  $i = 1, 2, 3, 4$  is

$$y_{k,i} = \arctan\left(\frac{p_{y,k} - s_{y,i}}{p_{x,k} - s_{x,i}}\right) + v_{k,i}, \quad (21)$$

where  $v_{k,i} \sim \mathcal{N}(0, 0.0036\text{rad}^2)$ .

The T-FoT approach was carried out in  $x$  and  $y$  dimensions individually, with a sliding time-window  $K$  no longer than one second. The polynomial T-FoT of order  $\gamma = 1$  is given as

$$\begin{cases} p_{x,t} = c_0^{(1)} + c_1^{(1)}t, \\ p_{y,t} = c_0^{(2)} + c_1^{(2)}t. \end{cases} \quad (22)$$

Given that the four sensors are of the same quality which is time-invariant (here we do not really need to know the statistics of  $v_{k,i}$ ), the joint optimization parameters at time  $k$  are estimated by

$$\underset{c_0^{(1)}, c_1^{(1)}, c_0^{(2)}, c_1^{(2)}}{\operatorname{argmin}} \sum_{t=k'}^k \sum_{i=1}^4 \left( y_{t,i} - \arctan\left(\frac{c_0^{(2)} + c_1^{(2)}t - s_{y,i}}{c_0^{(1)} + c_1^{(1)}t - s_{x,i}}\right) \right)^2.$$

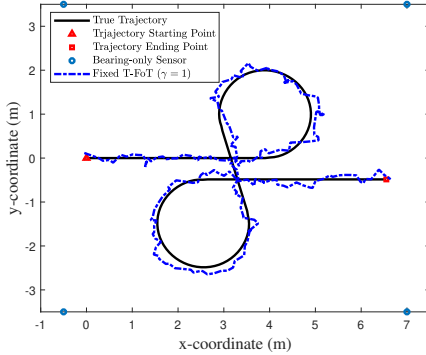
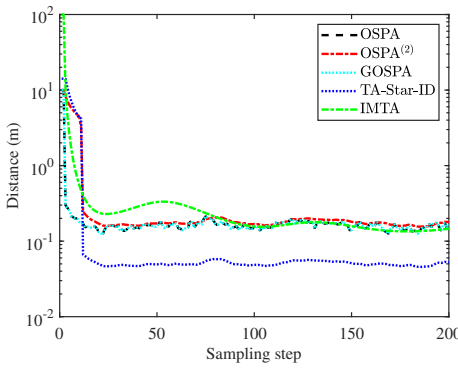


Fig. 6. The real trajectory of a maneuvering target and estimates in one trial.

Fig. 7. OSPA, OSPA<sup>(2)</sup>, GOSPA, TA-Star-ID and IMTA distance of the same T-FoT.

The T-FoT needs at least  $\gamma+1$  data points to start the fitting. Therefore, it cannot produce any estimate in the first sampling instant when  $\gamma = 1$ . Our fitting was performed from the second sampling instant and the first instant is treated as an MD. The simulation was performed for 100 runs, 200 sampling steps per run, based on the same trajectory (as shown in Fig. 6) but different observation realizations.

Based on the parameters given in Table II, the average OSPA, OSPA<sup>(2)</sup>, GOSPA, IMTA and TA-Star-ID over time are given in Fig. 7. First, the OSPA and GOSPA metrics demonstrate complete consistency, as the T-FoT accurately estimates the number of targets, i.e.,  $n - m = 0$  in both Eq. (3) and (4). The fluctuation in the TA-Star-ID over time complies with OSPA<sup>(2)</sup>, but is smaller and smoother than the

TABLE II  
METRIC PARAMETERS USED IN THE SINGLE TARGET SCENARIO

Parameters	Value Used	Metrics
$c$	10m	OSPA, OSPA <sup>(2)</sup> , GOSPA
$p$	2	
$\alpha$	2	GOSPA
$c_s$	10m	IMTA, (TA-)Star-ID
$c_t$	10m	

OSPA over time; the IMTA is the smoothest over time. This is simply because both the TA-Star-ID and OSPA<sup>(2)</sup>, as well as the IMTA, account for the trajectory-segment in the time-window rather than only the estimates at the newest time.

### B. Multiple Target In Presence of FA and MD

In this scenario, four targets moved with constant velocity in the area  $[-3, 9]\text{km} \times [-9, 15]\text{km}$ , as shown in Fig. 8. The starting and stopping positions for each trajectory are labeled with triangles and boxes, respectively. The existing intervals for their trajectories are  $[1, 100]\text{s}$ ,  $[10, 75]\text{s}$ ,  $[1, 90]\text{s}$  and  $[5, 85]\text{s}$ , respectively. As shown, the estimated T-FoTs are given by three polynomials. Target 4 that is assumed with very low detection probability is totally missed in all time.

The simulation is carried out for 100 Monte Carlo runs, each lasting 100s. Each target trajectory is modeled by a polynomial T-FoT with fixed order  $\gamma = 2$  as follows

$$F(t; \mathbf{C}) = \begin{bmatrix} c_0^{(1)}, c_1^{(1)}, c_2^{(1)} \\ c_0^{(2)}, c_1^{(2)}, c_2^{(2)} \end{bmatrix} \begin{bmatrix} 1 \\ t \\ t^2 \end{bmatrix}. \quad (23)$$

The measurements are made on the position T-FoT with measuring step size 1s and with additive, zero-mean Gaussian measurement noise as follows

$$\mathbf{y}_k = F(k; \mathbf{C}) + \mathbf{v}_k \quad (24)$$

where  $\mathbf{v}_k \sim \mathcal{N}(\mathbf{0}, 10000\text{m}^2)$ .

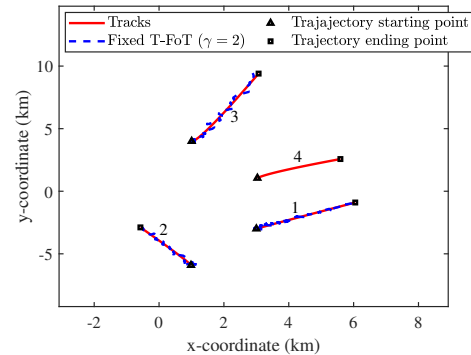
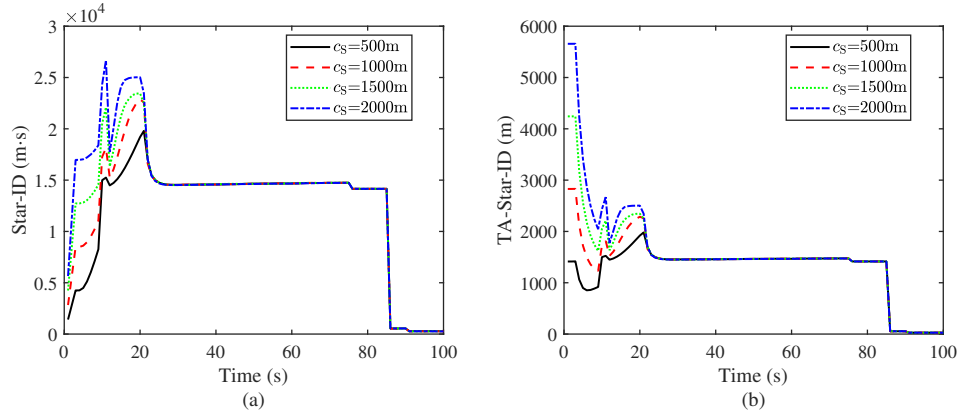
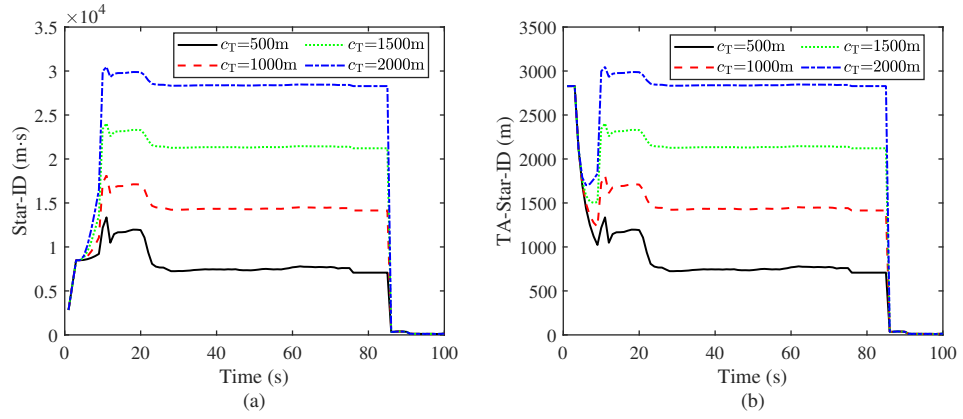


Fig. 8. 4 Targets move with constant velocity in the Cartesian coordinate.

We first set fixed  $c_t = 1\text{km}$  and different  $c_s$  (500m, 1km, 1.5km and 2km) to calculate the TA-Star-ID and Star-ID. As illustrated in Fig. 9 (a), the Star-ID increases with the increase of  $c_s$  over all when there is any segment MD or FA in the concerning time-window. Furthermore, both the Star-ID and the TA-Star-ID increase when new targets appear and decrease with their disappearance as they are basically cumulative distances summing up the errors regarding all target estimates.

We next fix  $c_s = 1\text{km}$  and set different  $c_t$  from 500m to 2km. As shown in Fig. 10, the TA-Star-ID and Star-ID consistently increase with the increase of  $c_t$  as long as there is TFA or TMD.

To conclude, it is confirmed that whatever  $c_s$  and  $c_t$  are, the Star-ID, but not the TA-Star-ID, basically increase with the growth of the sliding time-window at the initial stage since it is

Fig. 9. The effect of  $c_s$  on the Star-ID (a) and TA-Star-ID (b), respectively ( $c_T = 1\text{km}$ ).Fig. 10. The effect of  $c_T$  on the Star-ID (a) and TA-Star-ID (b), respectively ( $c_s = 1\text{km}$ ).

a distance integrating the errors in the whole time-window. In contrast, the TA-Star-ID shows the average T-FoT estimation error for each sampling period in the time-window, showing an average performance.

## VI. CONCLUSION

In this paper, we propose a metric for calculating the similarity between two arbitrary sets of continuous-time trajectories defined in the spatio-temporal domain, termed as the Star-ID. It associates and aligns the estimated and real trajectories in the spatio-temporal domain and distinguishes between the aligned and unaligned segments in calculating either localization integral distance or FA/MD penalties. Particularly, the time length is taken into account in the FA and MD penalties. The trajectory association depends on the Star-ID between two trajectories, which as well as the FA and MD cutoff coefficients is the prerequisite for calculating the Star-ID between two sets of multiple trajectories. Conditions that ensure the metric be a distance are specified and proven. Simulation in both single and multiple target tracking scenarios has demonstrated the effectiveness of the Star-ID and its time-averaged version. A valuable extension of the metric is to take into account the uncertainty or the existing probability of the estimated trajectories which may lead to better performance in both the tracklet association and distance calculation.

## APPENDIX

### A. Minkowski's inequality for T-FoT Sets

**Proposition 1.** Let  $d^{(\alpha)}(f, g)$  and  $d^{(\beta)}(f, g)$  denote two different metrics for measuring the distance between trajectories  $f(t)$  and  $g(t)$ . Given that both metrics satisfy the triangle inequality, i.e.,  $d^{(\alpha)}(f, g) \leq d^{(\alpha)}(f, h) + d^{(\alpha)}(h, g)$ ,  $d^{(\beta)}(f, g) \leq d^{(\beta)}(f, h) + d^{(\beta)}(h, g)$  for any trajectory  $h(t)$ , the new metric  $d^{(\alpha, \beta)}(f, g)$  defined as,  $1 \leq p < \infty$ ,

$$d^{(\alpha, \beta)}(f, g) \triangleq \left( d^{(\alpha)}(f, g)^p + d^{(\beta)}(f, g)^p \right)^{\frac{1}{p}}$$

satisfies the triangle inequality:

$$d^{(\alpha, \beta)}(f, g) \leq d^{(\alpha, \beta)}(f, h) + d^{(\alpha, \beta)}(h, g) \quad (25)$$

*Proof.* The proof is straightforward as follows

$$\begin{aligned} & d^{(\alpha, \beta)}(f, h) + d^{(\alpha, \beta)}(h, g) \\ &= (d^{(\alpha)}(f, h)^p + d^{(\beta)}(f, h)^p)^{\frac{1}{p}} + (d^{(\alpha)}(h, g)^p + d^{(\beta)}(h, g)^p)^{\frac{1}{p}} \\ &\geq \left( (d^{(\alpha)}(f, h) + d^{(\alpha)}(h, g))^p + (d^{(\beta)}(f, h) + d^{(\beta)}(h, g))^p \right)^{\frac{1}{p}} \end{aligned} \quad (26)$$

$$\begin{aligned} &\geq \left( d^{(\alpha)}(f, g)^p + d^{(\beta)}(f, g)^p \right)^{\frac{1}{p}} \\ &= d^{(\alpha, \beta)}(f, g) \end{aligned} \quad (27)$$

where the Minkowski's inequality <sup>2</sup> [42] was used in (26).  $\square$

### B. Proof of Theorem 1

Firstly, since  $d_{t_1, t_2}^{(p)}(f, g) \geq 0$ , when  $c_{\text{SFA}}, c_{\text{SMD}} > 0$ ,  $d_{\mathbf{c}}^{(p)}(f, g)$  satisfies non-negativity. Second, for any  $f, g$ , it is easy to see that  $d_{\mathbf{c}}^{(p)}(f, g) = 0$  if and only if  $f = g$ . Thus, the identity property is satisfied. Third, when  $c_{\text{SFA}} = c_{\text{SMD}}$  and  $c_{\text{TFA}} = c_{\text{TMD}}$ ,  $d_{\mathbf{c}}^{(p)}(\cdot, \cdot)$  is symmetric in its arguments, satisfying the third property.

Lastly, we prove the triangle inequality by starting from the following definition  $\bar{d}_{t_1, t_2}^{(c, p)}(f, g) \triangleq \min(d_{t_1, t_2}^{(p)}(f, g), r^{\frac{1}{p}}(c_{\text{SFA}} + c_{\text{SMD}})(t_2 - t_1))$ . It can be straightforwardly asserted that

$$d_{t_1, t_2}^{(c, p)}(f, g) = \left( \bar{d}_{t_1, t_2}^{(c, p)}(f, g) \right)^p. \quad (28)$$

Considering three T-FoTs  $f, g$  and  $h$  with time intervals denoted by  $T^{(f)} = [t_s^{(f)}, t_e^{(f)}]$ ,  $T^{(g)} = [t_s^{(g)}, t_e^{(g)}]$  and  $T^{(h)} = [t_s^{(h)}, t_e^{(h)}]$ , respectively, their joint temporal span of existence is  $T^{(f, h, g)} = [\min(t_s^{(f)}, t_s^{(g)}, t_s^{(h)}), \max(t_e^{(f)}, t_e^{(g)}, t_e^{(h)})]$ . Our proof is categorized into the following complementary cases:

Case 1:  $t_s^{(h)} < t_s^{(f)} < t_s^{(g)}, t_e^{(h)} < t_e^{(f)} < t_e^{(g)}$ ,

$$\begin{aligned} & d_{\mathbf{c}}^{(p)}(f, g) \\ &= \left( r \left( c_{\text{S}}(t_s^{(g)} - t_s^{(f)}) + c_{\text{S}}(t_e^{(g)} - t_e^{(f)}) \right)^p + d_{t_s^{(g)}, t_e^{(f)}}^{(c, p)}(f, g) \right)^{\frac{1}{p}} \\ &\leq \left( r \left( c_{\text{S}}(t_s^{(g)} - t_s^{(f)}) + c_{\text{S}}(t_e^{(g)} - t_e^{(f)}) \right)^p \right. \\ &\quad \left. + \left[ \bar{d}_{t_s^{(f)}, t_e^{(h)}}^{(c, p)}(f, g) + r^{\frac{1}{p}} c_{\text{S}}(t_e^{(f)} - t_e^{(h)}) \right]^p \right)^{\frac{1}{p}} \quad (29) \\ &\leq \left( r \left( c_{\text{S}}(t_s^{(g)} - t_s^{(f)}) + c_{\text{S}}(t_e^{(g)} - t_e^{(f)}) \right. \right. \\ &\quad \left. \left. + 2c_{\text{S}}(t_e^{(f)} - t_e^{(h)}) \right)^p + \left[ \bar{d}_{t_s^{(f)}, t_e^{(h)}}^{(c, p)}(f, g) \right]^p \right)^{\frac{1}{p}} \\ &\leq \left( r \left[ \left( c_{\text{S}}(t_s^{(f)} - t_s^{(h)}) + c_{\text{S}}(t_s^{(g)} - t_s^{(h)}) \right) \right. \right. \\ &\quad \left. \left. + \left( c_{\text{S}}(t_e^{(f)} - t_e^{(h)}) \right) + \left( c_{\text{S}}(t_e^{(g)} - t_e^{(h)}) \right) \right]^p \right. \\ &\quad \left. + \left[ \bar{d}_{t_s^{(f)}, t_e^{(h)}}^{(c, p)}(f, h) + \bar{d}_{t_s^{(g)}, t_e^{(h)}}^{(c, p)}(h, g) \right]^p \right)^{\frac{1}{p}} \quad (30) \\ &\leq \left( r \left( c_{\text{S}}(t_s^{(f)} - t_s^{(h)}) + c_{\text{S}}(t_e^{(f)} - t_e^{(h)}) \right)^p + d_{t_s^{(f)}, t_e^{(h)}}^{(c, p)}(f, h) \right)^{\frac{1}{p}} \\ &\quad + \left( r \left( c_{\text{S}}(t_s^{(g)} - t_s^{(h)}) + c_{\text{S}}(t_e^{(g)} - t_e^{(h)}) \right)^p + d_{t_s^{(g)}, t_e^{(h)}}^{(c, p)}(h, g) \right)^{\frac{1}{p}} \\ &= d_{\mathbf{c}}^{(p)}(f, h) + d_{\mathbf{c}}^{(p)}(h, g) \end{aligned}$$

<sup>2</sup>Given two sequences  $x = (\xi_1, \dots, \xi_n)$  and  $y = (\nu_1, \dots, \nu_n)$ , the Minkowski's inequality is defined as follows, for  $1 \leq p < \infty$ ,

$$\left( \sum_{i=1}^n |\xi_i + \nu_i|^p \right)^{\frac{1}{p}} \leq \left( \sum_{i=1}^n |\xi_i|^p \right)^{\frac{1}{p}} + \left( \sum_{i=1}^n |\nu_i|^p \right)^{\frac{1}{p}}$$

where (15) was used in (29) while Proposition 1 in (30).

$$\begin{aligned} & d_{\mathbf{c}}^{(p)}(f, h) \\ &= \left( r \left( c_{\text{S}}(t_s^{(f)} - t_s^{(h)}) + c_{\text{S}}(t_e^{(f)} - t_e^{(h)}) \right)^p + d_{t_s^{(f)}, t_e^{(h)}}^{(c, p)}(f, h) \right)^{\frac{1}{p}} \\ &\leq \left( r \left( c_{\text{S}}(t_s^{(f)} - t_s^{(h)}) + c_{\text{S}}(t_e^{(f)} - t_e^{(h)}) \right)^p \right. \\ &\quad \left. + \left[ \bar{d}_{t_s^{(g)}, t_e^{(h)}}^{(c, p)}(f, h) + r^{\frac{1}{p}} c_{\text{S}}(t_s^{(g)} - t_s^{(h)}) \right]^p \right)^{\frac{1}{p}} \quad (31) \end{aligned}$$

$$\begin{aligned} &\leq \left( r \left[ \left( c_{\text{S}}(t_s^{(g)} - t_s^{(f)}) + c_{\text{S}}(t_e^{(g)} - t_e^{(f)}) \right) \right. \right. \\ &\quad \left. \left. + \left( c_{\text{S}}(t_e^{(g)} - t_e^{(h)}) \right) + \left( c_{\text{S}}(t_s^{(g)} - t_s^{(h)}) \right) \right]^p \right. \\ &\quad \left. + \left[ \bar{d}_{t_s^{(g)}, t_e^{(h)}}^{(c, p)}(f, g) + \bar{d}_{t_s^{(g)}, t_e^{(h)}}^{(c, p)}(h, g) \right]^p \right)^{\frac{1}{p}} \\ &\leq \left( r \left( c_{\text{S}}(t_s^{(g)} - t_s^{(f)}) + c_{\text{S}}(t_e^{(g)} - t_e^{(f)}) \right)^p + d_{t_s^{(g)}, t_e^{(f)}}^{(c, p)}(f, g) \right)^{\frac{1}{p}} \\ &\quad + \left( r \left( c_{\text{S}}(t_s^{(g)} - t_s^{(h)}) + c_{\text{S}}(t_e^{(g)} - t_e^{(h)}) \right)^p + d_{t_s^{(g)}, t_e^{(h)}}^{(c, p)}(h, g) \right)^{\frac{1}{p}} \quad (32) \end{aligned}$$

$$= d_{\mathbf{c}}^{(p)}(f, g) + d_{\mathbf{c}}^{(p)}(h, g)$$

where (15) was used in (31) while Proposition 1 in (32).

$$\begin{aligned} & d_{\mathbf{c}}^{(p)}(h, g) \\ &= \left( r \left( c_{\text{S}}(t_s^{(g)} - t_s^{(h)}) + c_{\text{S}}(t_e^{(g)} - t_e^{(h)}) \right)^p + d_{t_s^{(g)}, t_e^{(h)}}^{(c, p)}(h, g) \right)^{\frac{1}{p}} \\ &\leq \left( r \left[ \left( c_{\text{S}}(t_s^{(f)} - t_s^{(h)}) \right) + \left( c_{\text{S}}(t_s^{(g)} - t_s^{(f)}) \right) \right. \right. \\ &\quad \left. \left. + \left( c_{\text{S}}(t_e^{(f)} - t_e^{(h)}) \right) + \left( c_{\text{S}}(t_e^{(g)} - t_e^{(f)}) \right) \right]^p \right. \\ &\quad \left. + \left[ \bar{d}_{t_s^{(f)}, t_e^{(h)}}^{(c, p)}(f, h) + \bar{d}_{t_s^{(g)}, t_e^{(f)}}^{(c, p)}(f, g) \right]^p \right)^{\frac{1}{p}} \\ &\leq d_{\mathbf{c}}^{(p)}(f, h) + d_{\mathbf{c}}^{(p)}(f, g) \quad (33) \end{aligned}$$

where Proposition 1 was used in (33).

This proves the triangle inequality for this case. The proof of the triangle inequality for the remaining cases 2-6 is analogous to that for case 1 and is omitted here.

- Case 2:  $t_s^{(h)} < t_s^{(g)} < t_s^{(f)}, t_e^{(h)} < t_e^{(f)} < t_e^{(g)}$ .
- Case 3:  $t_s^{(h)} < t_s^{(f)} < t_s^{(g)}, t_e^{(f)} < t_e^{(h)} < t_e^{(g)}$ .
- Case 4:  $t_s^{(h)} < t_s^{(g)} < t_s^{(f)}, t_e^{(f)} < t_e^{(h)} < t_e^{(g)}$ .
- Case 5:  $t_s^{(h)} < t_s^{(g)} < t_s^{(f)}, t_e^{(f)} < t_e^{(g)} < t_e^{(h)}$ .
- Case 6:  $t_s^{(h)} < t_s^{(g)} < t_s^{(f)}, t_e^{(f)} < t_e^{(g)} < t_e^{(h)}$ .

Summing up, we have now proved that the triangle inequality holds in all cases for  $d_{\mathbf{c}}^{(p)}(f, g)$ .

### C. Proof of Theorem 2

First, as proven in Theorem 1,  $d_{\mathbf{c}}^{(p)}(f, g)$  satisfies non-negativity while the rest part of  $d_{\mathbf{c}}^{(p)}(\mathcal{F}, \mathcal{G})$  is non-negative. So, the non-negativity property is therefore satisfied. Second, for  $f(t), g(t)$ , since  $d_{\mathbf{c}}^{(p)}(f, g) = 0$  if and only if  $f(t) = g(t)$ , then

$d_c^{(p)}(\mathcal{F}, \mathcal{G}) = 0$  if and only if  $\mathcal{F} = \mathcal{G}$ . Thus, the identity property is satisfied. Third, when  $c_{SFA} = c_{SMD}$  and  $c_{TFA} = c_{TMD}$ ,  $d_c^{(p)}(\cdot, \cdot)$  is symmetric in its arguments,  $d_c^{(p)}(\mathcal{F}, \mathcal{G})$  is also symmetric in its arguments, satisfying the third property. In what follows, we would like to prove the triangle inequality:

$$d_c^{(p)}(\mathcal{F}, \mathcal{G}) \leq d_c^{(p)}(\mathcal{F}, \mathcal{H}) + d_c^{(p)}(\mathcal{H}, \mathcal{G}) \quad (34)$$

Since this inequality is symmetric, we may assume without loss of generality that  $m \leq n$ . Our proof (given in the next page) addresses three complete and complementary cases differing in the relationship between  $m$ ,  $n$  and  $l$ . Proposition 1 was used in (35), (36) and (38). As shown in all these three cases, the triangle inequality (34) holds.

## REFERENCES

- [1] Y. Bar-Shalom, X.-R. Li, and T. Kirubarajan, *Estimation with Applications to Tracking and Navigation: Theory, Algorithms, and Software*. John Wiley & Sons, 2002.
- [2] S. Sarkka, *Bayesian Filtering and Smoothing*. New York, NY, USA: Cambridge University Press, 2013.
- [3] B.-N. Vo, M. Mallick, Y. Bar-Shalom, S. Coraluppi, R. Osborne, R. Mahler, and B.-T. Vo, "Multitarget tracking," in *Wiley Encyclopedia of Electrical and Electronics Engineering*. John Wiley & Sons, 2015.
- [4] S. Zhang, J. Wang, Z. Wang, Y. Gong, and Y. Liu, "Multi-target tracking by learning local-to-global trajectory models," *Pattern Recognit.*, vol. 48, no. 2, pp. 580–590, 2015.
- [5] B.-N. Vo, B.-T. Vo, and M. Beard, "Multi-sensor multi-object tracking with the generalized labeled multi-Bernoulli filter," *IEEE Trans. Signal Process.*, vol. 67, no. 23, pp. 5952–5967, 2019.
- [6] Á. F. García-Fernández, A. S. Rahmathullah, and L. Svensson, "A time-weighted metric for sets of trajectories to assess multi-object tracking algorithms," in *Proc. FUSION 2021*. Sun City, South Africa: IEEE, November 2021, pp. 1–8.
- [7] K. Di, T. Li, G. Li, Y. Song, and X. Dang, "Label matching: It is complicated," in *Proc. FUSION 2024*, Venice, Italy, 2024, pp. 1–8.
- [8] B. Ristic, B.-N. Vo, D. Clark, and B.-T. Vo, "A metric for performance evaluation of multi-target tracking algorithms," *IEEE Trans. Signal Process.*, vol. 59, no. 7, pp. 3452–3457, 2011.
- [9] P. Barrios, M. Adams, K. Leung, F. Inostroza, G. Naqvi, and M. E. Orchard, "Metrics for evaluating feature-based mapping performance," *IEEE Trans. Robot.*, vol. 33, no. 1, pp. 198–213, 2017.
- [10] T. Vu, "A complete optimal subpattern assignment (cospa) metric," in *Proc. FUSION 2020*, Rustenburg, South Africa, July 2020, pp. 1–8.
- [11] O. E. Drummond and B. E. Fridling, "Ambiguities in evaluating performance of multiple target tracking algorithms," in *Proc. SPIE*, vol. 1698, Orlando, FL, United States, August 1992, pp. 326 – 337.
- [12] B. Ristic, "A tool for track-while-scan algorithm evaluation," in *Proc. IDC 1999*, Adelaide, SA, Australia, February 1999, pp. 105–110.
- [13] S. Blackman and R. Popoli, "Design and analysis of modern tracking systems," *Norwood, MA: Artech House*, 1999.
- [14] R. L. Rothrock and O. E. Drummond, "Performance metrics for multiple-sensor multiple-target tracking," in *Proc. SPIE*, vol. 4048, Orlando, FL, United States, April 2000, pp. 521–531.
- [15] T. T. D. Nguyen, H. Rezatofighi, B.-N. Vo, B.-T. Vo, S. Savarese, and I. Reid, "How trustworthy are performance evaluations for basic vision tasks?" *IEEE Trans. Pattern Anal. Mach. Intell.*, vol. 45, no. 7, pp. 8538–8552, 2023.
- [16] D. Schuhmacher, B.-T. Vo, and B.-N. Vo, "A consistent metric for performance evaluation of multi-object filters," *IEEE Trans. Signal Process.*, vol. 56, no. 8, pp. 3447–3457, 2008.
- [17] S. Nagappa, D. E. Clark, and R. Mahler, "Incorporating track uncertainty into the ospa metric," in *Proc. FUSION 2011*, Chicago, IL, USA, July 2011, pp. 1–8.
- [18] X. He, R. Tharmarasa, T. Kirubarajan, and T. Thayaparan, "A track quality based metric for evaluating performance of multitarget filters," *IEEE Trans. Aerosp. Electron. Syst.*, vol. 49, no. 1, pp. 610–616, 2013.
- [19] J. Pinto, Y. Xia, L. Svensson, and H. Wyneersch, "An uncertainty-aware performance measure for multi-object tracking," *IEEE Signal Process. Lett.*, vol. 28, pp. 1689–1693, 2021.
- [20] A. S. Rahmathullah, Á. F. García-Fernández, and L. Svensson, "Generalized optimal sub-pattern assignment metric," in *Proc. FUSION 2017*. Xi'an, China: IEEE, July 2017, pp. 1–8.
- [21] A. F. García-Fernández, A. S. Rahmathullah, and L. Svensson, "A metric on the space of finite sets of trajectories for evaluation of multi-target tracking algorithms," *IEEE Trans. Signal Process.*, vol. 68, pp. 3917–3928, 2020.
- [22] B. Ristic, B.-N. Vo, and D. Clark, "Performance evaluation of multi-target tracking using the ospa metric," in *Proc. FUSION 2010*, Edinburgh, UK, July 2010, pp. 1–7.
- [23] T. Vu and R. Evans, "A new performance metric for multiple target tracking based on optimal subpattern assignment," in *Proc. FUSION 2014*, Salamanca, Spain, July 2014, pp. 1–8.
- [24] J. Bento and J. J. Zhu, "A metric for sets of trajectories that is practical and mathematically consistent," *CoRR*, vol. abs/1601.03094, 2016. [Online].
- [25] M. Beard, B. T. Vo, and B.-N. Vo, "A solution for large-scale multi-object tracking," *IEEE Trans. Signal Process.*, vol. 68, pp. 2754–2769, 2020.
- [26] D. Hu, L. Chen, H. Fang, Z. Fang, T. Li, and Y. Gao, "Spatio-temporal trajectory similarity measures: A comprehensive survey and quantitative study," *IEEE Trans. Knowl. Data Eng.*, vol. 36, no. 5, pp. 2191–2212, 2024.
- [27] H. Su, S. Liu, B. Zheng, X. Zhou, and K. Zheng, "A survey of trajectory distance measures and performance evaluation," *The VLDB Journal*, vol. 29, pp. 3–32, 2020.
- [28] M. Beard, B. T. Vo, and B.-N. Vo, "Ospa (2): Using the ospa metric to evaluate multi-target tracking performance," in *Proc. ICRAIS 2017*, Chiang Mai, Thailand, October 2017, pp. 86–91.
- [29] W. Talbot, J. Nubert, T. Tuna, C. Cadena, F. Dümbgen, J. Tordesillas, T. D. Barfoot, and M. Hutter, "Continuous-time state estimation methods in robotics: A survey," 2024. [Online].
- [30] Y. Xin, Y. Song, and T. Li, "A metric for multi-target continuous-time trajectory evaluation," in *Proc. ICRAIS 2022*, Hanoi, Vietnam, November 2022, pp. 364–370.
- [31] T. Li, H. Chen, S. Sun, and J. M. Corchado, "Joint smoothing and tracking based on continuous-time target trajectory function fitting," *IEEE Trans. Autom. Sci. Eng.*, vol. 16, no. 3, pp. 1476–1483, 2018.
- [32] T. Li, Y. Song, and H. Fan, "From target tracking to targeting track: A data-driven yet analytical approach to joint target detection and tracking," *Signal Process.*, vol. 205, p. 108883, 2023.
- [33] T. Li, Y. Song, G. Li, and H. Li, "From target tracking to targeting track — Part II: Regularized polynomial trajectory optimization," *Companion Paper, arXiv preprint*, 2025.
- [34] P. Furgale, T. D. Barfoot, and G. Sibley, "Continuous-time batch estimation using temporal basis functions," in *Proc. ICRA 2012*, Saint Paul, MN, USA, May 2012, pp. 2088–2095.
- [35] M. Pacholska, F. Dümbgen, and A. Scholefield, "Relax and recover: Guaranteed range-only continuous localization," *IEEE Robot. Autom. Lett.*, vol. 5, no. 2, pp. 2248–2255, 2020.
- [36] T. Li, J. Wang, G. Li, and D. Gao, "From target tracking to targeting track — Part III: Stochastic process modeling and online learning," *Companion Paper, arXiv preprint*, 2025.
- [37] H. Cramér, "On some classes of nonstationary stochastic processes," *Proceedings of the Fourth Berkeley Symposium on Mathematical Statistics and Probability*, vol. 2, pp. 57–78, 1961.
- [38] G. Urban and S. J. Koopman, *Time Series Analysis by State Space Methods*. Oxford: Oxford University Press, 2012.
- [39] P. Barrios and M. Adams, "A comparison of multi-object sub-pattern linear assignment metrics," in *Proc. ICRAIS 2023*, Hanoi, Vietnam, November 2023, pp. 712–718.
- [40] J. Munkres, "Algorithms for the assignment and transportation problems," *J. Soc. Ind. Appl. Math.*, vol. 5, no. 1, pp. 32–38, 1957.
- [41] J. Hartikainen, A. Solin, and S. Särkkä, "Optimal filtering with Kalman filters and smoothers a manual for the matlab toolbox EKF/UKF v.1.3," 2013.
- [42] C. S. Kubrusly, *Elements of operator theory*. Birkhäuser Boston, MA, 2011.

Case 1:  $m \leq n \leq l$

$$\begin{aligned}
d_{\mathcal{C}}^{(p)}(\mathcal{F}, \mathcal{G}) &\leq \left( \sum_{i=1}^n r (c_{\text{T}} T_{\text{TFA},i}^{\theta})^p + \sum_{j=1}^m \sum_{i=1}^n \mathbf{1}_{\theta}(f_j, g_i) \left( d_{\mathcal{C}}^{(p)}(f_j, g_i) \right)^p \right)^{\frac{1}{p}} \\
&\leq \left( \sum_{i=1}^n r (c_{\text{T}} T_{\text{TFA},i}^{\theta})^p + \sum_{j=1}^m \sum_{i=1}^l \left[ \mathbf{1}_{\theta}(f_j, h_i) \left( d_{\mathcal{C}}^{(p)}(f_j, h_i) \right) + \mathbf{1}_{\theta}(g_j, h_i) \left( d_{\mathcal{C}}^{(p)}(g_j, h_i) \right) \right]^p \right)^{\frac{1}{p}} \\
&\leq \left( \sum_{i=1}^n r (c_{\text{T}} T_{\text{TMD},i}^{\theta})^p + \sum_{i=1}^l r (c_{\text{T}} T_{\text{TFA},i}^{\theta})^p + \sum_{j=m+1}^n \sum_{i=1}^l \mathbf{1}_{\theta}(g_j, h_i) \left( d_{\mathcal{C}}^{(p)}(g_j, h_i) \right)^p \right. \\
&\quad \left. + \sum_{j=1}^m \sum_{i=1}^l \left[ \mathbf{1}_{\theta}(f_j, h_i) \left( d_{\mathcal{C}}^{(p)}(f_j, h_i) \right) + \mathbf{1}_{\theta}(g_j, h_i) \left( d_{\mathcal{C}}^{(p)}(g_j, h_i) \right) \right]^p \right)^{\frac{1}{p}} \\
&\leq \left( \sum_{i=1}^l r (c_{\text{T}} T_{\text{TFA},i}^{\theta})^p + \sum_{j=1}^m \sum_{i=1}^l \mathbf{1}_{\theta}(f_j, h_i) \left( d_{\mathcal{C}}^{(p)}(f_j, h_i) \right)^p \right)^{\frac{1}{p}} \\
&\quad + \left( \sum_{i=1}^n r (c_{\text{T}} T_{\text{TMD},i}^{\theta})^p + \sum_{j=1}^n \sum_{i=1}^l \mathbf{1}_{\theta}(g_j, h_i) \left( d_{\mathcal{C}}^{(p)}(g_j, h_i) \right)^p \right)^{\frac{1}{p}} \\
&= d_{\mathcal{C}}^{(p)}(\mathcal{F}, \mathcal{H}) + d_{\mathcal{C}}^{(p)}(\mathcal{G}, \mathcal{H})
\end{aligned} \tag{35}$$

Case 2:  $m \leq l \leq n$

$$\begin{aligned}
d_{\mathcal{C}}^{(p)}(\mathcal{F}, \mathcal{G}) &\leq \left( \sum_{i=1}^n r (c_{\text{T}} T_{\text{TFA},i}^{\theta})^p + \sum_{j=1}^m \sum_{i=1}^n \mathbf{1}_{\theta}(f_j, g_i) \left( d_{\mathcal{C}}^{(p)}(f_j, g_i) \right)^p \right)^{\frac{1}{p}} \\
&\leq \left( \sum_{i=1}^n r (c_{\text{T}} T_{\text{TFA},i}^{\theta})^p + \sum_{i=1}^l r (c_{\text{T}} T_{\text{TFA},i}^{\theta})^p + \sum_{j=1}^m \sum_{i=1}^n \left[ \mathbf{1}_{\theta}(f_j, h_i) \left( d_{\mathcal{C}}^{(p)}(f_j, h_i) \right) + \mathbf{1}_{\theta}(h_j, g_i) \left( d_{\mathcal{C}}^{(p)}(h_j, g_i) \right) \right]^p \right. \\
&\quad \left. + \sum_{j=m+1}^l \sum_{i=1}^n \mathbf{1}_{\theta}(h_j, g_i) \left( d_{\mathcal{C}}^{(p)}(h_j, g_i) \right)^p \right)^{\frac{1}{p}} \\
&\leq \left( \sum_{i=1}^l r (c_{\text{T}} T_{\text{TFA},i}^{\theta})^p + \sum_{j=1}^m \sum_{i=1}^l \mathbf{1}_{\theta}(f_j, h_i) \left( d_{\mathcal{C}}^{(p)}(f_j, h_i) \right)^p \right)^{\frac{1}{p}} \\
&\quad + \left( \sum_{i=1}^n r (c_{\text{T}} T_{\text{TFA},i}^{\theta})^p + \sum_{j=1}^l \sum_{i=1}^n \mathbf{1}_{\theta}(h_j, g_i) \left( d_{\mathcal{C}}^{(p)}(h_j, g_i) \right)^p \right)^{\frac{1}{p}} \\
&= d_{\mathcal{C}}^{(p)}(\mathcal{F}, \mathcal{H}) + d_{\mathcal{C}}^{(p)}(\mathcal{G}, \mathcal{H})
\end{aligned} \tag{36}$$

Case 3:  $l \leq m \leq n$

$$\begin{aligned}
d_{\mathcal{C}}^{(p)}(\mathcal{F}, \mathcal{G}) &\leq \left( \sum_{i=1}^n r (c_{\text{T}} T_{\text{TFA},i}^{\theta})^p + \sum_{j=1}^m \sum_{i=1}^n \mathbf{1}_{\theta}(f_j, g_i) \left( d_{\mathcal{C}}^{(p)}(f_j, g_i) \right)^p \right)^{\frac{1}{p}} \\
&\leq \left( \sum_{i=1}^n r (c_{\text{T}} T_{\text{TFA},i}^{\theta})^p + \sum_{i=1}^m r (c_{\text{T}} T_{\text{TFA},i}^{\theta})^p + \sum_{j=1}^l \sum_{i=1}^n \mathbf{1}_{\theta}(f_j, g_i) \left( d_{\mathcal{C}}^{(p)}(f_j, g_i) \right)^p \right)^{\frac{1}{p}}
\end{aligned} \tag{37}$$

$$\leq \left( \sum_{i=1}^n r (c_{\text{T}} T_{\text{TFA},i}^{\theta})^p + \sum_{i=1}^m r (c_{\text{T}} T_{\text{TFA},i}^{\theta})^p + \sum_{j=1}^l \sum_{i=1}^n \left[ \mathbf{1}_{\theta}(h_j, f_i) \left( d_{\mathcal{C}}^{(p)}(h_j, f_i) \right) + \mathbf{1}_{\theta}(h_j, g_i) \left( d_{\mathcal{C}}^{(p)}(h_j, g_i) \right) \right]^p \right)^{\frac{1}{p}} \tag{38}$$

$$\begin{aligned}
&\leq \left( \sum_{i=1}^m r (c_{\text{T}} T_{\text{TFA},i}^{\theta})^p + \sum_{j=1}^l \sum_{i=1}^m \mathbf{1}_{\theta}(h_j, f_i) \left( d_{\mathcal{C}}^{(p)}(h_j, f_i) \right)^p \right)^{\frac{1}{p}} \\
&\quad + \left( \sum_{i=1}^n r (c_{\text{T}} T_{\text{TFA},i}^{\theta})^p + \sum_{j=1}^l \sum_{i=1}^n \mathbf{1}_{\theta}(h_j, g_i) \left( d_{\mathcal{C}}^{(p)}(h_j, g_i) \right)^p \right)^{\frac{1}{p}} \\
&= d_{\mathcal{C}}^{(p)}(\mathcal{H}, \mathcal{F}) + d_{\mathcal{C}}^{(p)}(\mathcal{H}, \mathcal{G})
\end{aligned} \tag{38}$$

where (19) was used in (37).